**THE EUROPEAN
PHYSICAL JOURNAL D**

Regular Article

Observation of entanglement witnesses for orbital angular momentum states

M. Agnew[1], J. Leach[2,a], and R.W. Boyd[1,2]

[1] Dept. of Physics, University of Ottawa, 150 Louis Pasteur, K1N 6N5 Ottawa, Ontario, Canada
[2] Institute of Optics, University of Rochester, Rochester, 14627 New York, USA

Abstract. Entanglement witnesses provide an efficient means of determining the level of entanglement of a system using the minimum number of measurements. Here we demonstrate the observation of two-dimensional entanglement witnesses in the high-dimensional basis of orbital angular momentum (OAM). In this case, the number of potentially entangled subspaces scales as $d(d-1)/2$, where d is the dimension of the space. The choice of OAM as a basis is relevant as each subspace is not necessarily maximally entangled, thus providing the necessary state for certain tests of nonlocality. The expectation value of the witness gives an estimate of the state of each two-dimensional subspace belonging to the d-dimensional Hilbert space. These measurements demonstrate the degree of entanglement and therefore the suitability of the resulting subspaces for quantum information applications.

1 Introduction

Entanglement is a quantum mechanical phenomenon that results in non-local correlations that are stronger than any encountered in classical physics [1]. Due to this property, entanglement is extremely useful as a tool for quantum information protocols, such as quantum key distribution [2,3], quantum teleportation [4–6], and fundamental tests of quantum mechanics [7–9]. All of these applications rely on preserving the nature of the quantum state; however, a problem arises when the state interacts with its environment and the enhancement provided by quantum mechanics is lost. By characterising the state and modelling its interaction with the environment, we learn how best to take advantage of the enhancement provided by quantum physics. It is thus important to determine exactly the level of entanglement of a system in order to determine its suitability for such quantum information applications.

Quantum tomography is one approach to determine the exact density matrix of a quantum state [10–16]; however, tomography requires a large number of measurements, particularly for high-dimensional systems [16]. It is often not necessary to have the complete knowledge of the state that tomography provides. One alternative approach is the method of an entanglement witness [17–21], which has been experimentally realised in two dimensions [22] and in multipartite systems [23]. An entanglement witness does not determine the full state as in tomography, but it requires far fewer measurements to determine the

ᵃ e-mail: jonathan.leach@gmail.com

degree of entanglement. With only six measurements in a two-dimensional state space, an entanglement witness represents the fewest possible number of measurements that establishes whether or not the state is entangled.

In this paper, we demonstrate the first observation of entanglement witnesses for photons entangled in their orbital angular momentum (OAM). As the state space is multi-dimensional, there are many two-dimensional subspaces in which to observe entanglement. We use entanglement witnesses to test for entanglement in all possible two-dimensional subspaces belonging to a representative high-dimensional space of dimension $d = 41$.

2 Theory

During parametric downconversion, two photons are produced that possess equal and opposite OAMs and that are entangled in the OAM basis. The two-photon state is then

$$|\Psi\rangle = \sum_{\ell=-\infty}^{\infty} c_\ell |\ell\rangle_A \otimes |-\ell\rangle_B, \quad (1)$$

where $|c_\ell|^2$ denotes the probability that photon A is measured to have OAM $\ell\hbar$ and photon B is measured to have OAM $-\ell\hbar$.

Considering a state confined to a two-dimensional subspace, we obtain the state

$$|\Psi\rangle = \frac{1}{\sqrt{|c_{\ell_1}|^2 + |c_{\ell_2}|^2}} (c_{\ell_1}|\ell_1, -\ell_1\rangle + c_{\ell_2}|\ell_2, -\ell_2\rangle), \quad (2)$$
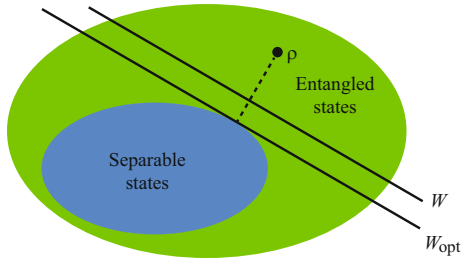
Fig. 1. (Color online) Schematic representation of an optimal entanglement witness. The state ρ is entangled and is separated from the set of separable states by both the entanglement witnesses W and W_{opt}. The optimal witness W_{opt} is tangent to the set of separable states.

where we use $|a, b\rangle$ to denote $|a\rangle_A \otimes |b\rangle_B$. Letting $\varepsilon = c_{\ell_2}/c_{\ell_1}$, we obtain the nonmaximally entangled state

$$|\Psi_\varepsilon\rangle = \frac{1}{\sqrt{1 + |\varepsilon|^2}} \left(|\ell_1, -\ell_1\rangle + \varepsilon |\ell_2, -\ell_2\rangle \right). \qquad (3)$$

Here ℓ_1 and ℓ_2 can take any value in the range $-[d/2]$ to $[d/2]$ for the dimension d in which the measurement is taken, where $[x]$ is the integer part of x. When ε is equal to zero, the state is separable; when ε is equal to unity, the state is maximally entangled. The density matrix for this state is

$$\rho_\varepsilon = \frac{1}{1 + |\varepsilon|^2} \begin{pmatrix} 0 & 0 & 0 & 0 \\ 0 & 1 & \varepsilon^* & 0 \\ 0 & \varepsilon & |\varepsilon|^2 & 0 \\ 0 & 0 & 0 & 0 \end{pmatrix}, \qquad (4)$$

where we use the basis vectors $|\ell_1, -\ell_2\rangle$, $|\ell_1, -\ell_1\rangle$, $|\ell_2, -\ell_2\rangle$, and $|\ell_2, -\ell_1\rangle$.

An entanglement witness W is an operator that indicates whether or not a particular state is entangled. A state ρ_{ent} is entangled if and only if $\text{Tr}(W\rho_{\text{ent}}) < 0$, while $\text{Tr}(W\rho_{\text{sep}}) \geq 0$ for any separable state ρ_{sep} [24]. A visualisation of the role of an entanglement witness is shown in Figure 1.

While many entanglement witnesses may be appropriate for a certain entangled state, one particular type is an optimal entanglement witness. An optimal entanglement witness W_{opt} is one for which there is no other witness that can detect all states detected by W_{opt} [17]. In other words, W_{opt} is tangent to the set of separable states S.

There are several methods of constructing entanglement witnesses [17,25,26]. In this work, we use a standard optimal entanglement witness for a state ρ with nonpositive partial transpose. The general form of the optimal entanglement witness is

$$W = (|\eta\rangle\langle\eta|)^{T_B}, \qquad (5)$$

where X^{T_B} denotes the partial transpose of X on the Hilbert space belonging to photon B, and $|\eta\rangle$ denotes the eigenvector that corresponds to the minimum eigenvalue of ρ^{T_B}.

For the specific case of the density matrix ρ_ε in equation (4) where ε is real and positive, the eigenvector corresponding to the minimum eigenvalue of $\rho_\varepsilon{}^{T_B}$ is

$$|\eta\rangle = \frac{1}{\sqrt{2}} \left(|\ell_2, -\ell_1\rangle - |\ell_1, -\ell_2\rangle \right). \qquad (6)$$

Using equation (5), we obtain for the state (4) the following entanglement witness:

$$W = \frac{1}{2} \begin{pmatrix} 1 & 0 & 0 & 0 \\ 0 & 0 & -1 & 0 \\ 0 & -1 & 0 & 0 \\ 0 & 0 & 0 & 1 \end{pmatrix}. \qquad (7)$$

This entanglement witness is the same irrespective of the level of entanglement present, i.e. regardless of the value of ε.

To measure the entanglement witness, we can decompose the operator into its constituent local measurements. A two-dimensional operator in the OAM basis can be described by the following decomposition [18]:

$$\begin{aligned}
W = \; &\alpha^2 |z_1^+ z_2^-\rangle\langle z_1^+ z_2^-| + \beta^2 |z_2^+ z_1^-\rangle\langle z_2^+ z_1^-| \\
&+ \alpha\beta(|x_A^+ x_B^+\rangle\langle x_A^+ x_B^+| + |x_A^- x_B^-\rangle\langle x_A^- x_B^-| \\
&- |y_A^+ y_B^-\rangle\langle y_A^+ y_B^-| - |y_A^- y_B^+\rangle\langle y_A^- y_B^+|),
\end{aligned} \qquad (8)$$

where $|z_1^\pm\rangle = |\pm\ell_1\rangle$, $|z_2^\pm\rangle = |\pm\ell_2\rangle$, $|x_A^\pm\rangle = \frac{1}{\sqrt{2}} (|\ell_1\rangle \pm |\ell_2\rangle)$, $|x_B^\pm\rangle = \frac{1}{\sqrt{2}} (|-\ell_1\rangle \pm |-\ell_2\rangle)$, $|y_A^\pm\rangle = \frac{1}{\sqrt{2}} (|\ell_1\rangle \pm i|\ell_2\rangle)$, and $|y_B^\pm\rangle = \frac{1}{\sqrt{2}} (|-\ell_1\rangle \pm i|-\ell_2\rangle)$. The choice of $\alpha = 1/\sqrt{2}$ and $\beta = -1/\sqrt{2}$ corresponds to the decomposition of the particular witness of equation (7). The resulting decomposition contains six terms, thus requiring six direct measurements to establish the level of entanglement of any two-dimensional subspace.

Since the number of two-dimensional subspaces in any d-dimensional system is the binomial coefficient $\binom{d}{2}$, the total number of measurements required to determine the number of entangled subspaces within such a system is

$$N = 6\binom{d}{2} = 6\frac{d!}{2!(d-2)!} = 3d(d-1). \qquad (9)$$

For $d = 41$, this requires only $N = 4290$, which takes approximately 24 h for a 20 s integration time. For comparison, tomography for the entire $d = 41$ space would require $N = d^4 - 1 = 2\,825\,760$, which would take approximately two years for the same integration time [16].

3 Experiment

We use a frequency-tripled Nd:YAG laser at 355 nm to pump a 3-mm-long type I BBO crystal; see Figure 2. This parametric downconversion process generates photon pairs entangled in the transverse degree of freedom, as in equation (1). We use spatial light modulators (SLMs) coupled to single-mode fibres to make projective measurements of the quantum state of each of these photons. The SLM converts the desired measurement state to
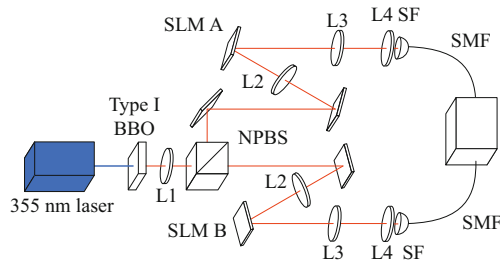
Fig. 2. (Color online) Experimental setup. L1 = 300 mm, L2 = 750 mm, L3 = 1000 mm, L4 = 3.2 mm, SLM = spatial light modulator, NPBS = non-polarising beam splitter, SF = 710 ± 5 nm spectral filter, SMF = single-mode fiber.
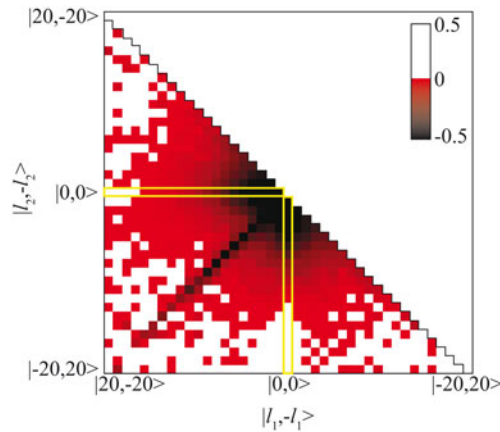

Fig. 3. (Color online) Expectation value of the entanglement witness of equation (7). The intensity axis indicates the expectation value resulting from the subspace of the form (3), where $|\ell_1, -\ell_1\rangle$ is the state indicated on the horizontal axis and $|\ell_2, -\ell_2\rangle$ is the state indicated on the vertical axis. Subspaces with $\ell_1 = 0$ or $\ell_2 = 0$ are outlined in yellow. The subspaces above the black line are redundant and thus not shown.

the fundamental state by displaying a computer-generated hologram to modify the phase, thus creating an effective means of mode selection. The detection is done using two avalanche photo detectors (APDs) connected to a coincidence counting card with resolution of 25 ns. The coincidence counts are converted into probabilities by dividing the coincidences for a given subspace by the sum of the counts measured in that subspace.

4 Results and discussion

We have obtained the expectation value of the entanglement witness for all two-dimensional subspaces within a $d = 41$ dimension state space. As shown in Figure 3, this produces for each subspace a value that lies in the range −0.5 to 0.5. Any non-negative value indicates a separable subspace, while the magnitude of a negative result indicates how entangled that subspace is. The lowest values, i.e. the most entangled subspaces, are found in subspaces with low ℓ_1 and ℓ_2 (which have high signal-to-noise ratio) and along the line where $\ell_1 = -\ell_2$ (which are the maximally entangled states).
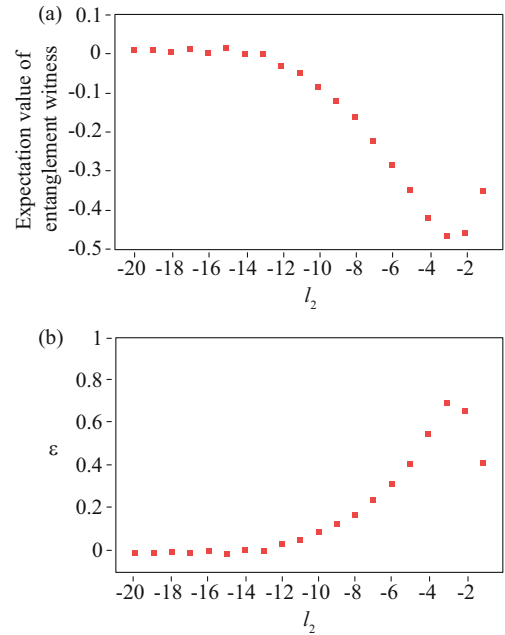

Fig. 4. (Color online) (a) The experimental expectation values of the entanglement witness on the states of equation (12), with ℓ_2 shown on the horizontal axis. (b) The level of entanglement ε calculated from the expectation values.

However, the normalisation method outlined above results in falsely low values for some states with high ℓ. These are considered to be outliers, which occur because of the normalisation within the subspace. At very high ℓ, there is very low signal, and thus any coincidences that occur due to noise will be normalised to a high probability, resulting in the illusory indication of an entangled subspace. This phenomenon begins to occur where $|\ell_1| = |\ell_2| > 12$, as seen in Figure 3.

In the following section, we show how the expectation value of the witness gives an estimate of the state of each two-dimensional subspace. This general result allows us to characterise the degree of entanglement in our particular system.

For the case where c_{ℓ_2} and c_{ℓ_1} are real-valued, as in this experiment, we can determine the expectation value of the entanglement witness for any subspace described by equation (3). Using equations (4) and (7), one can calculate the expectation value as

$$\mathrm{Tr}(\rho_\varepsilon W) = \langle W \rangle = -\frac{\varepsilon}{1 + \varepsilon^2}. \tag{10}$$

Solving for ε, we find

$$\varepsilon = \frac{c_{\ell_2}}{c_{\ell_1}} = \frac{\sqrt{1 - 4\langle W \rangle^2} - 1}{2\langle W \rangle}. \tag{11}$$

Using this result, we can determine the approximate value of ε and therefore the level of entanglement of a subspace.

The data in the vertical yellow-outlined box in Figure 3 is shown in Figure 4a. These values correspond to the states

$$|\Psi\rangle = \frac{1}{\sqrt{1 + \varepsilon^2}} \left(|0, 0\rangle + \varepsilon |\ell_2, -\ell_2\rangle \right), \tag{12}$$
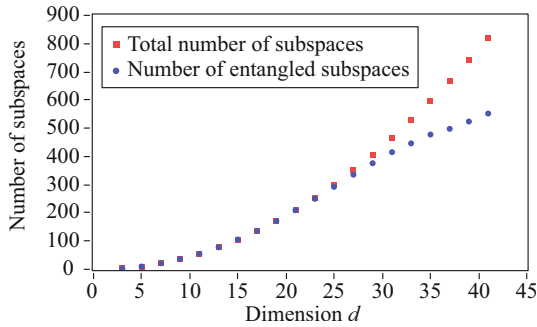
Fig. 5. (Color online) The number of entangled subspaces (circles) and total subspaces (squares) for odd dimensions.

that is, states for which $\ell_1 = 0$. Thus the degree of entanglement ε is simply c_{ℓ_2}/c_0. Since c_0 is equal to unity, this reduces to simply c_{ℓ_2}.

The calculated degree of entanglement $\varepsilon = c_{\ell_2}$ for each of these states is shown in Figure 4b. As expected, the degree of entanglement ε increases as ℓ_2 decreases, which means that lower-dimensional subspaces are more entangled than higher-dimensional subspaces. This is known to be the case based on previous investigations of the spiral bandwidth, which is the range of ℓ over which $|c_\ell|^2$ is nonzero [27–29].

The experimentally measured value of the entanglement witness depends on both the generated state and our ability to detect it. The projective measurements that are key to this experiment use computer-generated holograms that have symmetries that change according to their constituent modes. A consequence is that our detection capabilities include a sensitivity to modal dependent alignment errors, which can introduce crosstalk for particular measurements. Further investigation may be required to separate the interplay between the contributions of the generated state and modal detection capabilities of the projective measurements.

Taking the number of subspaces with negative expectation value, we can obtain an estimate of how many entangled subspaces there are. The number of entangled subspaces is shown in Figure 5, along with the total number of subspaces in each dimension. The two curves are approximately the same until $d \approx 25$, or $\ell \approx \pm 12$. Thus beginning at $|\ell| = 12$, some subspaces are not entangled.

5 Conclusion

We have demonstrated the use of entanglement witnesses for two-dimensional subspaces of photons entangled in a high-dimensional OAM basis. We have used this data to determine the degree of entanglement of these subspaces and thus their suitability for use in quantum information science. This result represents the first measurement of entanglement for high-dimensional OAM systems with the minimum number of measurements. This is an important step towards the use of these states in quantum protocols, where it is often necessary to efficiently test the degree of entanglement.

References

1. M.D. Reid, P.D. Drummond, W.P. Bowen, E.G. Cavalcanti, P.K. Lam, H.A. Bachor, U.L. Andersen, G. Leuchs, Rev. Mod. Phys. **81**, 1727 (2009)
2. A.K. Ekert, Phys. Rev. Lett. **67**, 661 (1991)
3. N. Gisin, G. Ribordy, W. Tittel, H. Zbinden, Rev. Mod. Phys. **74**, 145 (2002)
4. C.H. Bennett, G. Brassard, C. Crépeau, R. Jozsa, A. Peres, W.K. Wootters, Phys. Rev. Lett. **70**, 1895 (1993)
5. D. Bouwmeester, J.W. Pan, K. Mattle, M. Eibl, H. Weinfurter, A. Zeilinger, Nature **390**, 575 (1997)
6. I. Marcikic, H. de Riedmatten, W. Tittel, H. Zbinden, N. Gisin, Nature **421**, 509 (2003)
7. A. Einstein, B. Podolsky, N. Rosen, Phys. Rev. **47**, 777 (1935)
8. J.S. Bell, Physics **1**, 195 (1964)
9. L. Hardy, Phys. Rev. Lett. **71**, 1665 (1993)
10. D.F.V. James, P.G. Kwiat, W.J. Munro, A.G. White, Phys. Rev. A **64**, 052312 (2001)
11. N.K. Langford, R.B. Dalton, M.D. Harvey, J.L. OBrien, G.J. Pryde, A. Gilchrist, S.D. Bartlett, A.G. White, Phys. Rev. Lett. **93**, 053601 (2004)
12. G. Molina-Terriza, A. Vaziri, J. Řeháček, Z. Hradil, A. Zeilinger, Phys. Rev. Lett. **92**, 167903 (2004)
13. K.J. Resch, P. Walther, A. Zeilinger, Phys. Rev. Lett. **94**, 070402 (2005)
14. D.N. Matsukevich, P. Maunz, D.L. Moehring, S. Olmschenk, C. Monroe, Phys. Rev. Lett. **100**, 150404 (2008)
15. B. Jack, J. Leach, H. Ritsch, S.M. Barnett, M.J. Padgett, S. Franke-Arnold, New J. Phys. **11**, 103024 (2009)
16. M. Agnew, J. Leach, M. McLaren, F.S. Roux, R.W. Boyd, Phys. Rev. A **84**, 062101 (2011)
17. M. Lewenstein, B. Kraus, J.I. Cirac, P. Horodecki, Phys. Rev. A **62**, 052310 (2000)
18. O. Gühne, P. Hyllus, D. Bruß, A. Ekert, M. Lewenstein, C. Macchiavello, A. Sanpera, Phys. Rev. A **66**, 062305 (2002)
19. G.M. D'Ariano, C. Macchiavello, M.G.A. Paris, Phys. Rev. A **67**, 042310 (2003)
20. A.O. Pittenger, M.H. Rubin, Phys. Rev. A **67**, 012327 (2003)
21. R.A. Bertlmann, K. Durstberger, B.C. Hiesmayr, P. Krammer, Phys. Rev. A **72**, 052331 (2005)
22. M. Barbieri, F. De Martini, G. Di Nepi, P. Mataloni, G.M. D'Ariano, C. Macchiavello, Phys. Rev. Lett. **91**, 227901 (2003)
23. M. Bourennane, M. Eibl, C. Kurtsiefer, S. Gaertner, H. Weinfurter, O. Gühne, P. Hyllus, D. Bruß, M. Lewenstein, A. Sanpera, Phys. Rev. Lett. **92**, 087902 (2004)
24. M. Horodecki, P. Horodecki, R. Horodecki, Phys. Lett. A **223**, 1 (1996)
25. M. Lewenstein, B. Kraus, P. Horodecki, J.I. Cirac, Phys. Rev. A **63**, 044304 (2001)
26. D. Bruß, J.I. Cirac, P. Horodecki, F. Hulpke, B. Kraus, M. Lewenstein, A. Sanpera, J. Mod. Opt. **49**, 1399 (2002)
27. J.P. Torres, A. Alexandrescu, L. Torner, Phys. Rev. A **68**, 050301 (2003)
28. F.M. Miatto, A.M. Yao, S.M. Barnett, Phys. Rev. A **83**, 033816 (2011)
29. A.M. Yao, New J. Phys. **13**, 053048 (2011)